(Received 25 October 2023, Accepted 2 January 2024, Scheduled 20 January 2024)

A Novel of Metamaterial Ultra Compact Reconfigurable Phase Shifter Based on Dual Composite Right Left Handed Structure (D-CRLH)

Yasser Sobhy Farag[1,*], Mohamed Abaza[1], and Ahmed Fawzy Daw[2]

[1]*Electronics and Communications Engineering Department*
Arab Academy for Science, Technology and Maritime Transport, Giza, Egypt
[2]*Electronics and Communications Department, MSA University, Giza, Egypt*

ABSTRACT: A novel ultra-compact dual-band reconfigurable microstrip phase shifter designed by using a dual-composite right/left handed D-CRLH technique of metamaterial is introduced. The paper proposes detailed studies between the simulation and the fabricated prototype results. Moreover, the study of the proposed phase shifter explains a shifting range from 0° till 360° by submitting four mounted surface switches in different spots of the fingers. Switches have fixed states shifting to provide the controlling of the requested range. The switches were chosen to be from PIN Diode as it has many compatible characteristics which are explained in the proposed paper. The reconfigurable phase shifter designed with high quality factors and low insertion loss 0.25 and 0.2 at 5.7 GHz and 7.5 GHz respectively with a very compact size area 8×11. The proposed shifter supports the application of wide band usage especially for network access point, Wi-Fi, WiMAX network, and wireless LAN connections in addition to the application of point to point microwave radio links and X-band of satellite & space communications.

1. INTRODUCTION

Recently, microstrip phase shifter becomes an essential point of the researches on electromagnetic field especially ultra-wide band. Ultra-wideband is an essential point in the research of electromagnetic field because of its critical uses in many fields of various communication systems such as radar communications [1], wireless network applications [2], satellite communications [3], phased array antenna [4], military devices [5], medical uses as well as its intervention in many optical applications and many others [6]. The proposed phase shifter could be defined by a module of two ports that reposition the input signal phase to convey it with a new alternative adaptation in its angle in the phase of output signal while keeping a magnitude of signal amplitude constant without varying [7], as any change in the amplitude value is considered as a loss and named insertion loss of the device [8].

In view of this research, the main aspect that revolves around this topic is designing by metamaterial as it will be the hub of this paper. It is known that any general engineering researches aim to get the most benefit at the lowest cost especially in RF and microwave engineering researches, and metamaterial fulfils this goal [9]. It produces a microstrip design about five times smaller than the normal with very low consuming power, as well as it generates a trivial insertion loss for the output [10]. Moreover, metamaterial presents remarkable increase in output gain and enhancement in output band width [11]. To sum up, we can abridge that the usage of metamaterial makes a divergence of reduction of the cost with very high quality in results which means a big effect in microstrip market, thus many institutions have made investments in researches of metamaterial components like medical sector, military institutions, optical researches, and many others as they saw that the future of manufacturing of next era of microstrip would be by metamaterial [12–15].

This paper will introduce a novel microstrip phase shifter with a reconfigurable structure to allow varying the phase shifting cycle from 0° to 360° with a starting step 5.625° for each band to not restrict the module in only one shifting phase. This could be designed with four definite switches mounted in fingers of the structure to allow the module flexible to switch the shifting process smoothly. The design is distinguished by its very miniaturized size area $8 \times 11\,\text{mm}^2$ and operates in dual bands at 5.7 GHz & 7.5 GHz with very low insertion losses 0.25 and 0.2, respectively. The structure is designed by using metamaterial especially D-CRLH technique that allows to operate in wideband with applications of ultra-higher bands.

2. METHODOLOGY

Firstly, the design structure is based on a single cell from conducting material and grounded with a conducting surface layer of height 0.3 under the substrate that act as low impedance which reduces the noise and reflects the radio waves from other integrated devices. The cell is centred by a mender line that connected input & output port to balance the inductance effect

* Corresponding author: Yasser Sobhy Farag (Y.abdelsl30429@student.aast.edu).

TABLE 1. Values of dimensions of the structure layout.

Parameter	Length (mm)	Parameter	Length (mm)
d1	**1.1**	**h1**	**0.8**
d2	**0.2**	**h2**	**5**
d3	**1.5**	**h3**	**0.6**
d4	**4.6**	**h4**	**3**

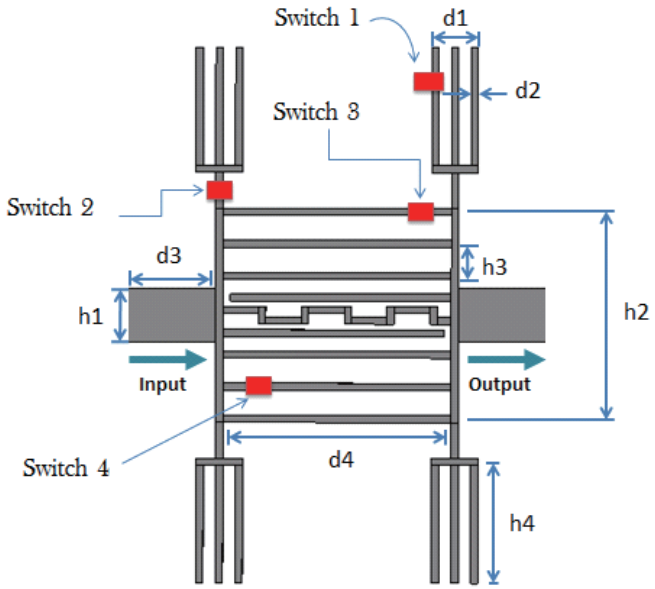

FIGURE 1. Layout dimensions of the structure.

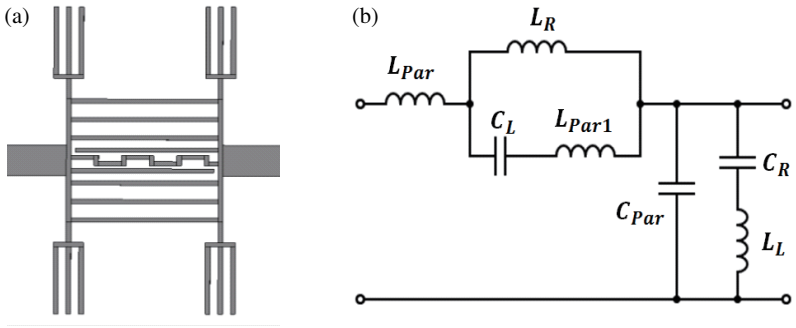

FIGURE 2. (a) Schematic cell and (b) Equivalent π-model for D-CRLH-TL unit cell.

of the device as shown in Figure 1. Furthermore, there are three fingers states up and down for each side, and each of them acts as single inductor parallel with each other. Besides that, two opened fingers surrounded the mender line for the capacitance effect which acts as two capacitors parallel to each other shunt with mender line. Additionally, the design is provided by four forks with three fingers for each that applies the equiponderance for the inductance and admittance for the device as it acts as three shunt capacitors series with one inductor for each fork. Table 1 shows the numerical analysis for each length of the design with clarifying entrance of the input signal as well as the dimensions of the signal path for each finger till the output port, in addition to the spots that mounted the switches on.

3. D-CRLH PHASE SHIFTER CELL THEORY & SIMULATION

The dual composite right left handed (DCRLH) metamaterial technique was extracted from the well-known CRLH-TL type. It consists of a reversed version of CRLH technique of metamaterial, constructed with series parallel LC tank and followed by a shunt series LC tank as shown in the π-model circuit of the design [16].

The introduced design in this section employed a D-CRLH phase shifter using one cell structure to reach dual bands, as shown in Figure 2(b) π-model, and the unit cell of shifter consists of LC parallel series with a parasitic inductor for

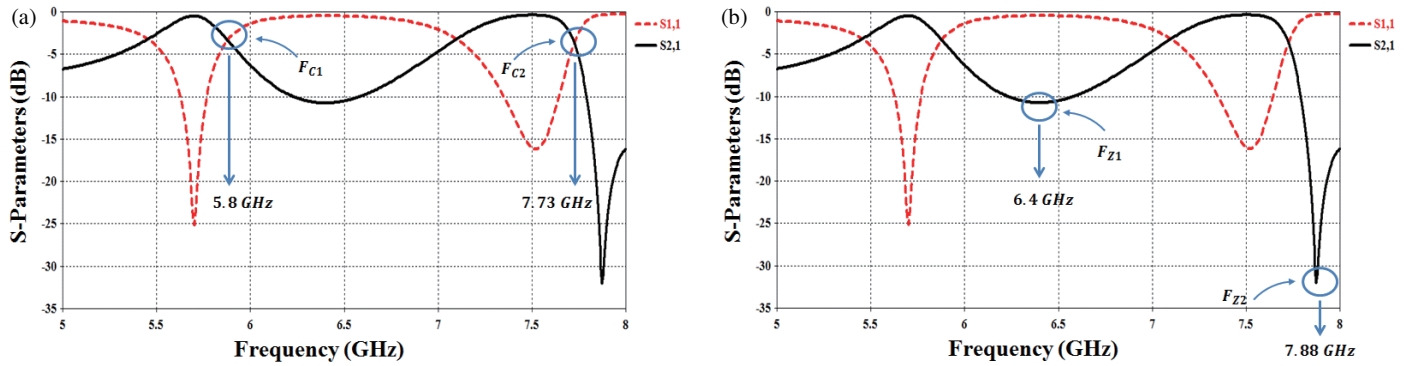

FIGURE 3. (a) Simulation of S-parameters and cut of frequencies (All switches OFF). (b) Simulation of S-parameters and zeroes frequencies.

impedance effect and LC series shunted with parasitic capacitor for admittance. Furthermore, D-CRLH cell is coupled to both input and output ports through a horizontally mender line in the middle as shown in Figure 2(a). For the design of Figure 2, we can analyze the cut-off frequency mathematically when using the dispersion spread equation [17] by:

$$\cos\beta d = 1 + \frac{1}{2}ZY \tag{1}$$

where,

$$Z = Z_1 + \frac{Z_2 Z_3}{Z_2 + Z_3}, \quad Z_1 = j\omega L_{Par} \tag{2}$$

$$Z_2 = j\omega L_{Par1} + \frac{1}{j\omega C_L}, \quad \text{and} \quad Z_3 = j\omega L_R$$

$$Y = Y_1 + Y_2, \quad Y_1 = j\omega C_{Par}, \quad \text{and} \tag{3}$$

$$Y_2 = \frac{1}{(j\omega L_L) + \left(\frac{1}{j\omega C_R}\right)}$$

The cut-off frequencies (F_{c1} and F_{c2}), in this case, when substituting $\beta d = \pi$ in (1) where β is a propagation constant; Z is the total impedance; Y is the total admittance; L_{Par} and C_{Par} are parasitic inductance and capacitance respectively; L_L and C_L are values of left handed inductance and capacitance, respectively; L_R and C_R are values of right handed inductance and capacitance, respectively. Assuming that C_{Par} is neglected as it is a very small value compared with other values of the rest of capacitors. Thus, cut-off frequencies could be extracted as:

$$-4 = \left(\frac{j\omega L_R\left(1-\omega^2 L_{Par}C_L\right)}{1-\omega^2(L_R+L_{Par})C_L}\right)\left(\frac{j\omega C_R}{1-\omega^2 L_L C_R}\right)\pi \mid F$$

$$= 5.8 \text{ GHz},\ 7.73 \text{ GHz} \tag{4}$$

On the other hand, the condition of the zero frequencies (F_{Z1} and F_{Z2}) could be analyzed when the scattering parameter S_{21} is substituted by the value of zero:

$$S_{21} = \left(\frac{2}{A + D + \frac{B}{Z_0} + CZ_0} \mid F = 6.4 \text{ GHz},\ 7.88 \text{ GHz}\right) = 0 \tag{5}$$

where,

$$A = 1 + ZY$$

$$A = 1 + \left(j\omega L_{Par1} + \frac{j\omega L_R\left(1-\omega^2 L_{Par1}C_L\right)}{1-\omega^2(L_R+L_{Par1})C_L}\right)\left(\frac{j\omega C_R}{1-\omega^2 L_L C_R}\right) \tag{6}$$

$$B = Z = \left(j\omega L_{Par1} + \frac{j\omega L_R\left(1-\omega^2 L_{Par1}C_L\right)}{1-\omega^2(L_R+L_{Par1})C_L}\right) \tag{7}$$

$$C = Y = \left(\frac{j\omega C_R}{1-\omega^2 L_L C_R}\right) \tag{8}$$

$$D = 1 \tag{9}$$

It is supposed that the mathematical analysis of zero frequencies could be present when the impedance and admittance are substituted with ∞ value in (2) and (3), respectively, thus for $Z = \infty$, the first zero frequency could be calculated by [23]:

$$F_{Z1} = \frac{1}{2\pi\sqrt{(L_{Par1} + L_R)C_L}} \tag{10}$$

On the other hand, after substituting $Y = \infty$ the second zero could be calculated by:

$$F_{Z2} = \frac{1}{2\pi\sqrt{L_L C_R}} \tag{11}$$

On the basis of the prior analysis from (4) to (11), assuming that all parasitic values are neglected and substitute F_{c1} and F_{c2} with frequency 5.8 GHz and 7.73 GHz respectively as well as F_{Z1} and F_{Z2} with frequency 6.4 GHz and 7.88 GHz respectively, all the values of lumped components are $\mathbf{L_R} = \mathbf{1.4}$ nH, $\mathbf{C_L} = \mathbf{0.45}$ pF, $\mathbf{L_L} = \mathbf{1.3}$ nH, $\mathbf{C_R} = \mathbf{0.35}$ pF.

After explaining the layout dimensions and the theory of the cell, the simulation results for the device are presented with explaining cut-off frequencies and zeros frequencies in the result of Figures 3(a) and (b). Firstly, CST simulator is used to simulate S-parameters of the device, as it started with a normal case of the device with all switches OFF to simulate the input reflection coefficient that represents S_{11} parameter, also the voltage forward gain that represents S_{21}. It is shown that the reflection coefficient is less than -10 dB for each frequency band, and the insertion losses are 0.2 & 0.25 for the dual frequencies 5.7 GHz and 7.5 GHz respectively in addition to 0.15 GHz & 0.3 GHz as bandwidth for each respectively.

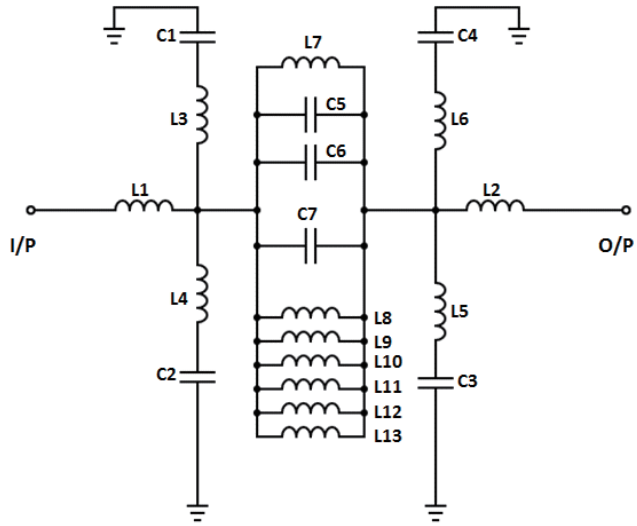

FIGURE 4. Equivalent circuit schematic.

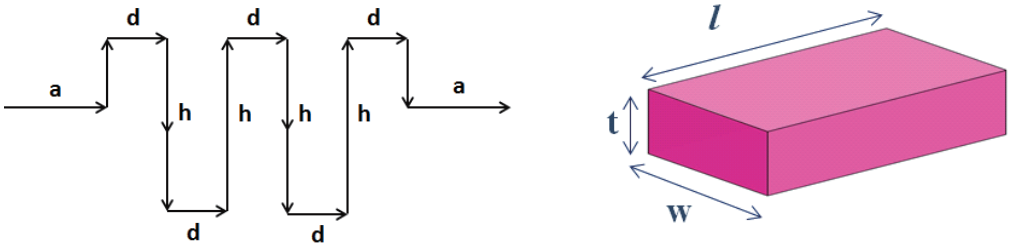

FIGURE 5. Mender line dimensions explanation.

4. D-CRLH PHASE SHIFTER EQUIVALENTS CIRCUIT

In order to comprehend the suggested phase shifter structure, the conversion of microstrip strip design to LC model is very important to dedicate the study of the structure. Assuming that the transmission lines of the microstrip are lossless material, the LC model topology could be analyzed as $\mathbf{L_1}$, $\mathbf{L_2}$, $\mathbf{L_3}$, $\mathbf{L_4}$, $\mathbf{L_5}$, $\mathbf{L_6}$, $\mathbf{L_8}$, $\mathbf{L_9}$, $\mathbf{L_{10}}$, $\mathbf{L_{11}}$, $\mathbf{L_{12}}$, and $\mathbf{L_{13}}$ which represent the inductances of all transmission lines in the design, and $\mathbf{L_7}$ is considered as the inductance of mender line. $\mathbf{C_1}$, $\mathbf{C_2}$, $\mathbf{C_3}$, $\mathbf{C_4}$ represent the capacitance effect of the fingers of each fork, and $\mathbf{C_5}$ and $\mathbf{C_6}$ represent the capacitance effect of the gap between the trips inside the cell. Finally $\mathbf{C_7}$ represents the interdigital capacitor between centralized mender line and the surrounded open strips.

As shown, Figure 4 illustrate the equivalent circuit for the D-CRLH phase shifter. The circuit started and ended with two inductors equivalent to the two ports, with each inductor connected with two inductor series with capacitor that represent each fork. All are connected with main interdigital capacitor which symbolizes the capacitance effect around the mender line. Interdigital capacitor is shunted with two capacitors which represent the two open fingers. The two capacitors are parallel with six inductors which represent all other fingers of the cell. Finally, all the previous capacitors and inductors are parallel to the initial inductor; this inductor represents the main mender line that centralized the structure.

Hereunder below, the analysis for each passive element in the circuit:

Firstly, all inductors in the circuit except mender line inductor of the middle could be calculated from the equation below that represents the equation of inductance in microstrip device with a difference of their compensations [18]:

$$L = \frac{Z}{\omega}\tan(\beta l) \tag{12}$$

Here $\beta = \frac{2\pi}{\lambda_g}$, where $\lambda_g = \frac{C}{\sqrt{\epsilon_{eff}}f}$, Z represents the impedance of the finger of entrance the signal, $\omega = 2\pi f$, and C is speed of light. On the other hand, the equation of the meander line inductor $\mathbf{L_7}$ could be calculated by [19]:

$$L_{mender\ line} = 2L_a + 2L_b + NL_h + (N+1)L_d \tag{13}$$

where L of each mender line is [20]:

$$L = 0.002l\left(\frac{\ln[2l]}{(w+t)} + 0.50049 + \frac{(w+t)}{3l}\right) \tag{14}$$

where $\mathbf{w}$ and $\mathbf{t}$ are dimensions of the cross-section as shown in Figure 5; $\mathbf{L_a}$, $\mathbf{L_b}$, $\mathbf{L_h}$, $\mathbf{L_d}$ are self-inductances of segments, where the length is $l = a, b, h, d$ (respectively), as represented in Figure 5, which are calculated by means of the expression for self-inductance (12). In Equation (13), N represents the number of segments of the greatest length h of the finger, and

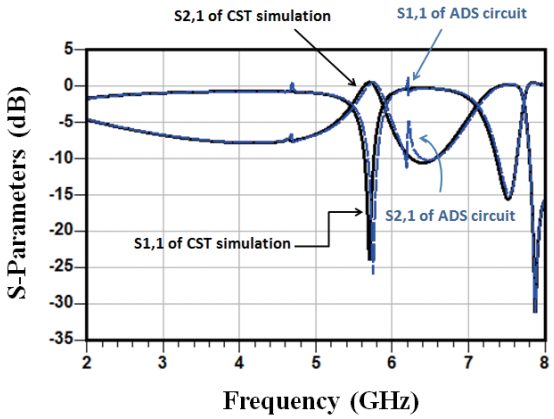

FIGURE 6. Integration of the microstrip CST simulation results and circuit ADS simulation.

TABLE 2. Values of passive elements in the equivalent circuit.

Component	L_1	L_2	L_3	L_4	L_5	L_6	L_7
Value/nH	3.65	3.65	0.14	0.14	0.14	0.14	0.83
Component	L_8	L_9	L_{10}	L_{11}	L_{12}	L_{13}	
Value/nH	2.05	2.05	2.05	2.05	2.05	2.05	
Component	C_1	C_2	C_3	C_4	C_5	C_6	C_7
Value/pF	4.7	4.7	4.7	4.7	14.2	14.2	3.8

t represents the height of the mender line cube. On the other hand, all capacitors in the circuit except C_7 could be calculated with the equation:

$$C = \frac{d\epsilon_0}{A} \tag{15}$$

where d is the length of the finger, and A represents the area of the proposed finger. Otherwise, C_7 stands for the interdigital capacitor and will be calculated with [21]:

$$C \approx (\epsilon_r + 1)[(N-3)A1 + A2] * l\,(\text{pF}) \tag{16}$$

where

$$A1 = 4.409\tanh\left(0.55\left[\frac{\mathbf{h}}{\mathbf{w}}\right]^{0.45}\right) * 10^2\,(\text{pF}/\mu\text{m}) \tag{17}$$

$$A2 = 9.92\tanh\left(0.52\left[\frac{\mathbf{h}}{\mathbf{w}}\right]^{0.5}\right) * 10^2\,(\text{pF}/\mu\text{m}) \tag{18}$$

where **h** is the height of the finger, **w** the width of the finger, and N the number of turns of the mender line. After calculating all passive components of the circuit, Table 2 shows the numerical results for each passive component in the circuit.

To inspect the operation of the proposed structure, the equivalent circuit of the design is emulated by ADS simulation program. From the representation of Figure 6, it could be seen that ADS simulation results present a very good agreement with CST simulation of the layout structure. Moreover, they are very close in their insertion loss results and their bandwidth which means that the structure is designed very precisely by calculating the LC model.

5. D-CRLH RECONFIGURATION SWITCHING PROCESS

Primarily, the design consists of four PIN diodes which were put in various places on the fingers of the surface structure to lead the shifting of the phase of the input signal as shown in Figure 7. Four pin diodes provide the incursion of the phase from 0° to 360° by four bits for each band frequency. Firstly, the incursion of the frequency is divided into two stages; in the first place for the frequency of 5.7 GHz, the four switches shift the frequency with four bits with initial step 5.625°, moreover with second step 45°, furthermore with 60° degree step, with final step of 270°. On the other hand, the other passband is 7.5 GHz with also 4-bits shifting, starting with 5.625° step, along with 11.25° step, in addition to 30° step, finally ends with 110° shifting step. Hereunder the phase shift steps simulation results for each switch in the dual bands.

Figures 8(a), (b), (c), (d) illustrate the simulation form of the four switches corresponding to first passband 5.7 GHz. On the other hand, Figures 8(e), (f), (g), (h) present the shifting states of the other band 7.5 GHz. The simulation represents the phase difference between the standard phase and the switched phase. For example, Figure 8(a) shows that the first switch is in ON state, and all the rest are in the OFF state, then input signals shift firstly with 5.625° in 5.7 GHz band and 5.625° also in 7.5 GHz band. After that, switch 2 is at the ON state, and the rest are at in the OFF state, thus the input signal is shifted by 45° in 5.7 GHz band and 11.25° in 7.5 GHz band as shown in Figures 8(b), (f), respectively. Figure 8 describes how the selected switches could shift the input signal with recognized state for

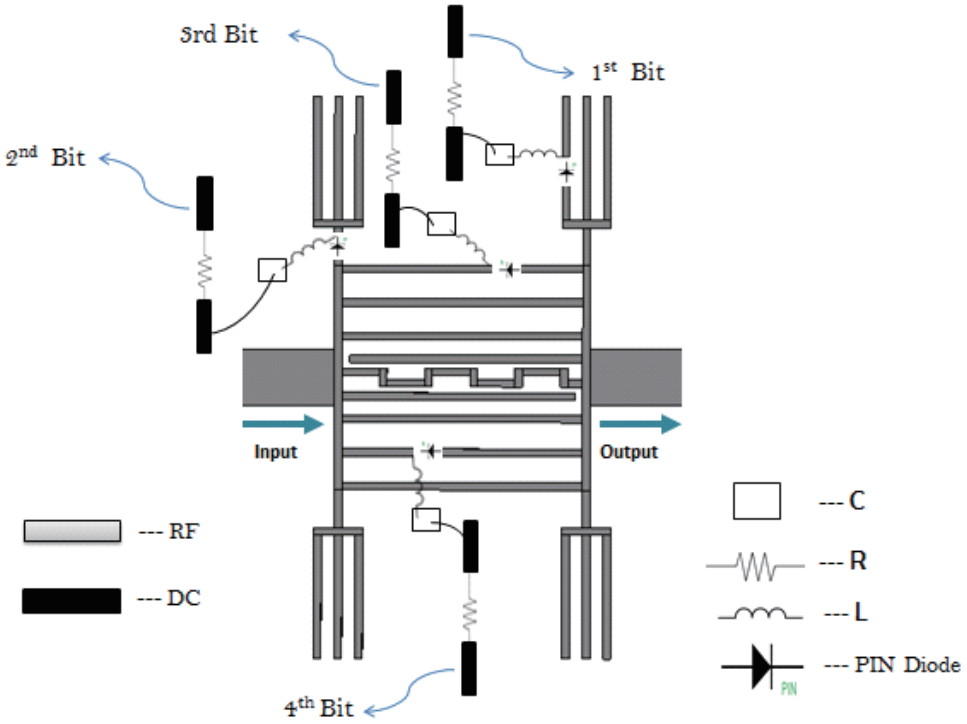

FIGURE 7. Layout of 4-bit phase-shifter module.

each band to reach the 360° shifting flexible by the proposed switches.

6. FABRICATION & HARDWARE RESULTS

The suggested phase shifter prototype was fabricated on a Rogers Duorid RT5880 substrate with dielectric constant $\varepsilon_r = 2.2$ and thickness $h = 0.38$ mm, and the size area of the fabricated shifter is measured by 8 mm $\times$ 11 mm. The scattering parameters are measured with real fabrication by Rohde & Schwarz ZVL20 network analyzer. Figure 11 represents the comparison between the fabricated and simulated results. Based on the fabricated results, the measurement of the fabricated insertion loss is 0.26 and 0.22 at 5.7 GHz and at 7.5 GHz, respectively. The introduced result integration shows a good agreement between the simulated and measured. Figure 9 represents the face surface structure for the fabricated design without mounting the switches.

The structure is designed to be in reconfigurable states by using switches to achieve the proposed states. Figure 11 presents the face of the circuit of the structure with mounted pin diodes drilled on the stubs of the fingers of the shifter. Infineon BAR64 PIN Diode is used to obtain the ON and OFF states for the shifter. The choice of this diode depends on many attributes that distinguish from the other diodes, as it has high range frequency up to 8 GHz. The diode has single configuration with maximum forward current 150 mA in addition to maximum reverse voltage 150 V. Moreover, the diode has typical carrier time life (TCTL) 1550 ns with diode capacitance 0.35 pF. The pin diodes are mounted on the surface of the metal patch essentially on four varying fingers to achieve proposed shifting states in each frequency band. Furthermore, Murata chip capacitor and coilcraft chip inductor were used as lumped elements integrated with pin diodes as they have high self-resonance frequency greater than the operating frequencies, and SMA-connectors were used for measuring realistic S-parameters. Figure 10 presents the comparison between the real fabricated results and ADS simulation in normal state.

Finally ADS program is used to integrate and present all the fabricated shifting results as shown in Figures 12 and 13. The black solid line represents the result of S_{21} in the normal state of real shifting result. On the other hand, the rest of doted lines represent the results of S_{21} after shifting which depends on its switch. All lines are shown with the real results and real shifting after fabrication. The results show a very good agreement with the previous simulated phase shifting results.

7. COMPARISON WITH RELATED WORK

The comparison between the proposed work and the relative past works, as well as the advantage and disadvantage for the proposed work, will be discussed in this section. The fabricated diplexer is distinguished from all other past works in Table 3 with novelty in its size, because using metamaterial in design made a big difference in the size of its dimensions compared with any other work. On the other hand, the technique of D-CRLH allows the proposed shifter to operate in dual bands which lack in other works. Furthermore, using metamaterial distinguishes the results of the proposed work with the lowest insertion loss from others. Moreover, it did not lose the feature

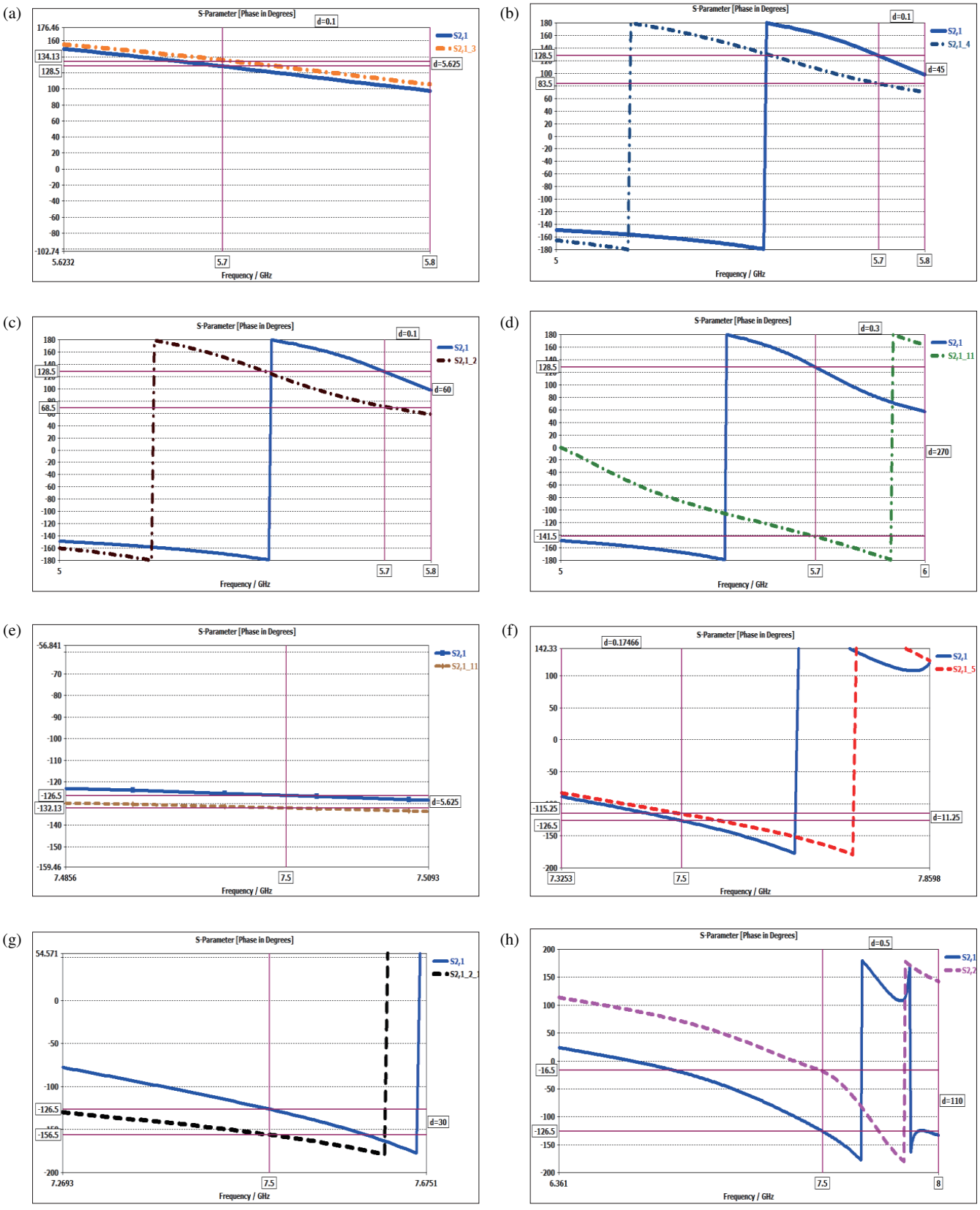

FIGURE 8. (a) Switch 1 with shifting step 5.625° in 5.7 GHz band. (b) Switch 2 with shifting step 45° in 5.7 GHz band. (c) Switch 3 with shifting step 60° in 5.7 GHz band. (d) Switch 4 with shifting step 270° in 5.7 GHz band. (e) Switch 1 with shifting step 5.625° in 7.5 GHz band. (f) Switch 2 with shifting step 11.25° in 7.5 GHz band. (g) Switch 3 with shifting step 30° in 7.5 GHz band. (h) Switch 4 with shifting step 110° in 7.5 GHz band.

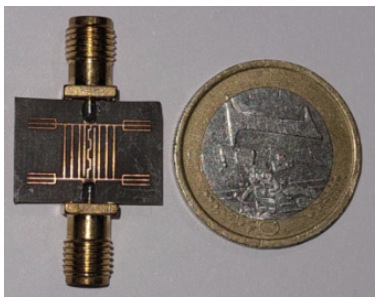

FIGURE 9. Layout fabricated structure on normal state.

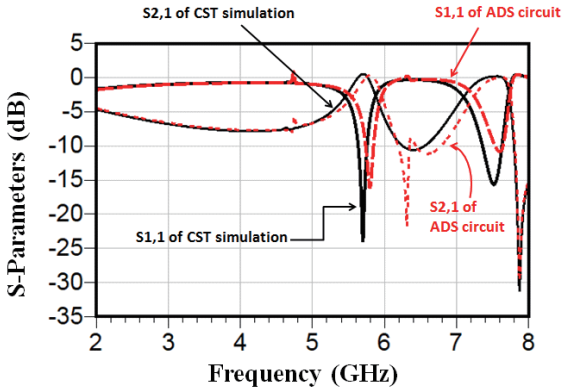

FIGURE 10. Integration of the microstrip CST simulation results and real fabricated results on normal state.

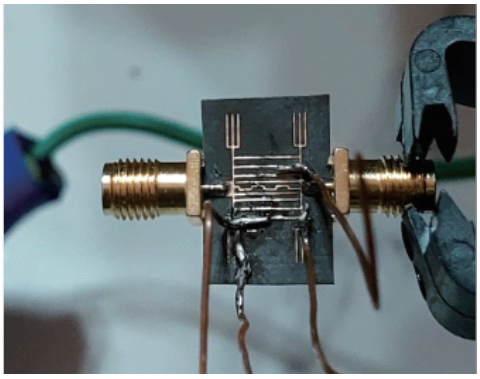

FIGURE 11. Photograph of 4-bit phase shifter module.

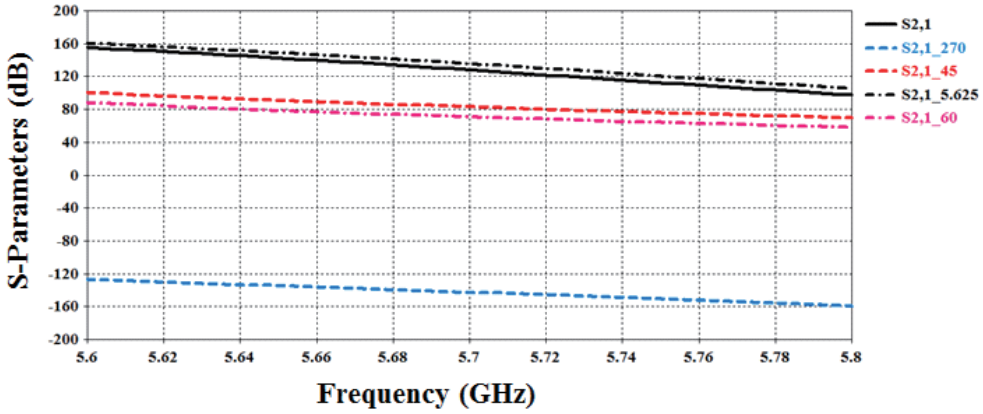

FIGURE 12. Integration results of shifting of real results of band frequency 5.7 GHz.

of phase range from 0° to 360° like [23, 24, 26]. Finally, the comparison shows superiority in the dimensions of the tradeoff relation of any design from the size, cost, and output performance compared to other related past works.

8. ADVANTAGE, DISADVANTAGE AND FUTURE WORK

This section will introduce a brief discussion on advantage and disadvantage for the proposed work with the plan of the discussed future work. The most distinctive feature of this design is its small size that makes its very cheap compared with the normal costs of microstrip phase shifters. Moreover, the operation of the module in ultra-wideband makes its application very wide in many different fields like radar communications, wireless network applications, X-band of satellite, and space communications, as well as other applications in optical and military network communications. The main advantage for the

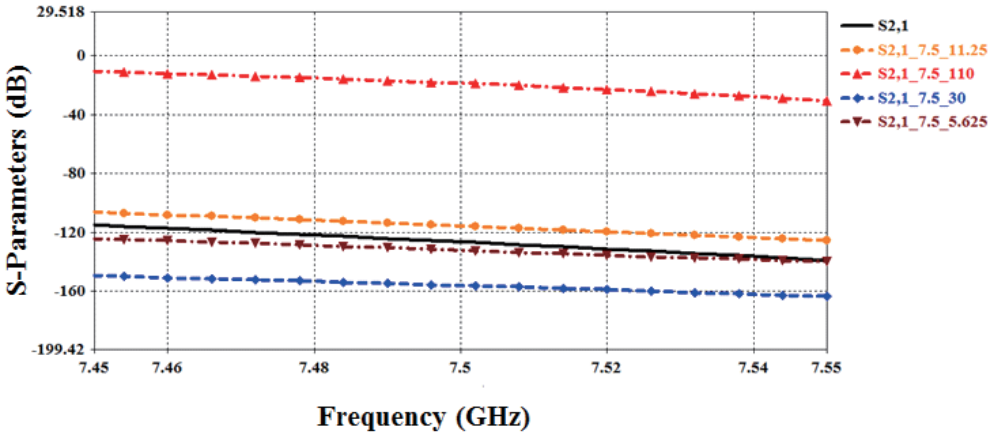

FIGURE 13. Integration results of shifting of real results of band frequency 7.5 GHz.

TABLE 3. Comparison between propose work with past related work.

Phase shifter	Frequency (GHz)	Phase Range	Insertion Loss (dB)	Reconfigurable Design	Size (mm)
Proposed shifter	5.7/7.5 (dual band)	0° to 360°	0.25/0.2	YES	8 × 11
Ref. [2] (2022)	4.75 to 5.25 (mono band)	0° to 360°	2.04	YES	10 × 40
Ref. [23] (2023)	6.5 (mono band)	0° to 270°	0.35	YES	30 × 40
Ref. [24] (2023)	16.5 to 31 (mono wide range)	0° to 180°	7.2	YES	25 × 30
Ref. [25] (2023)	2 to 2.8 (mono band)	0° to 360°	0.33	NO	40 × 40
Ref. [26] (2023)	5 to 6 (mono band)	0° to 180°	0.48	YES	18 × 22

proposed work is producing the highest power gain around 99% with very low insertion loss 0.2/0.25 dB for each band, and using metamaterial technique helps to miniaturize the structure into the lowest dimensions for phase shifter in market. Moreover, the ability to operate in dual bands allows to use the module in many applications in the mean time, adding to that the reconfigurability of the design by using switches that make the shifter more tunable with many phases from 0° to 360° by fixed steps starting from 5.625° for each band. Finally, the proposed structure provides a nearly ideal idea for researchers from the size, performance, cost, and applications. On the other hand, the comment of disadvantage for the proposed design is choosing the type of pin diode used as switches. Despite the benefits of miniaturizing the size of structure, it is very difficult to choose the type of pin diode, and this type is rare to find in market easily with the proposed characteristics. Thus, the discussed future plan is to convert the analogue control for tuning by pin diodes with full control with a embedded system by replacing diodes with RF MEMS and connect them with external microcontroller. It will provide many features such as low consumption for power control, very compact size for controlling circuit, and precision, and reliability.

9. CONCLUSION

An efficient structure of microstrip reconfigurable phase shifter based on DCRLH metamaterial technique is introduced. The structure that supports dual bands of ultra-wideband at 5.7 GHz and 7.5 GHz has very low insertion loss 0.25 and 0.2 for each band respectively as well as high power efficiency. Furthermore, the design supports reconfigurability by switching states with mounting pin diodes as switches on the surface structure of the design. Switches make the design to shift the real band with 4 states for each band to reach the 0° to 360° shifting process with the initial step phase by 5.625° for each band. The design presents a novelty in structure size for a reconfigurable microstrip phase shifter as the structure is measured by a compact dimensions 8 mm × 11 mm. Finally, the results of scattering parameters and shifting band of fabrication design were measured by Rohde and Schwarz-ZVL20 Network tester which present an excellent match with the results of simulation and equivalent circuit with future plan to convert the controlling circuit with embedded system and replacing switches with RF MEMS and analogue circuit with programmable microcontroller.

REFERENCES

[1] Bilal, A., A. Quddious, A. Kanno, T. Kawanishi, M. A. Antoniades, and S. Iezekiel, "1-bit reconfigurable phase shifter for mm-wave antenna beam-steering applications," in *2023 IEEE International Symposium on Antennas and Propagation and USNC-URSI Radio Science Meeting (USNC-URSI)*, 1643–1644, 2023.

[2] Tamura, J. and H. Arai, "A broadband reflection-type phase shifter with low loss variation using magic-T and anti-phase reflection loads," in *2023 IEEE/MTT-S International Microwave Symposium-IMS2023*, 1054–1057, 2023.

[3] Bilal, A., A. Quddious, A. Kanno, T. Kawanishi, M. A. Antoniades, and S. Iezekiel, "Fixed-length arbitrary-phase tunable NRI-TL metamaterial phase shifter for antenna beam-steering applications," in *2023 17th European Conference on Antennas and Propagation (EuCAP)*, 1–4, 2023.

[4] Wang, J. and Y. Yan, "Mechanical tuning phase shifter based on adjustable substrate," *IEICE Electronics Express*, 2023.

[5] Gouda, A. and S. Ghosh, "An analytical study of curved frequency selective surfaces for shielding applications," *Microwave and Optical Technology Letters*, Vol. 65, No. 12, 3139–3146, 2023.

[6] Sarmah, K., R. Konch, and S. Goswami, "Metamaterial CSRR loaded T-junction phase shifting power divider operating at 2.4 GHz," *Advances in Intelligent Computing and Communication*, Vol. 430, 339, 2022.

[7] Hammad, Y. T., M. A. Abdalla, and A. F. Daw, "A compact band stop filter with sharp stopband response using D-CRLH configuration," in *2018 12th International Congress on Artificial Materials for Novel Wave Phenomena (Metamaterials)*, 004–006, 2018.

[8] Shao, W., B. Yang, H. Kamada, and N. Shinohara, "Aperture-coupled beam-scanning patch array with parasitic elements using a reconfigurable series-fed phase-shifting structure," *IEEE Antennas and Wireless Propagation Letters*, Vol. 22, No. 7, 1617–1621, 2023.

[9] Daw, A. F., P. A. Fawzey, and M. N. Adly, "Quad-band resonator depends on CRLH/D-CRLH structures," *Microwaves & RF*, Oct. 2019.

[10] Al-Omari, M., H. Attia, K. K. Qureshi, and S. I. M. Sheikh, "Design of frequency-reconfigurable antenna on dielectric and magnetic metamaterial composite substrate," *IEEE Antennas and Wireless Propagation Letters*, Vol. 22, No. 4, 943–947, 2022.

[11] Barowski, J., L. Schmitt, K. Kother, and M. Hoffmann, "Design, simulation, and characterization of MEMS-based slot waveguides," *IEEE Transactions on Microwave Theory and Techniques*, Vol. 71, No. 9, 3819–3828, 2023.

[12] Deng, J., P. Burasa, and K. Wu, "Compact 140–220 GHz E/H waveguide phase shifter and its application to terahertz multiport circuits," *IEEE Transactions on Terahertz Science and Technology*, Vol. 13, No. 5, 511–525, 2023.

[13] Koul, S. K. and S. Dey, "Micromachined phase shifters," *Micromachined Circuits and Devices*, Vol. 859, 155, 2022.

[14] Gao, X., W. Y. Cui, Z. Gu, J. Zhang, Y. Ren, Q. Ma, and T. J. Cui, "Multi-mode and reconfigurable phase shifter of spoof surface plasmons," *IEEE Transactions on Antennas and Propagation*, Vol. 71, No. 6, 5361–5369, 2023.

[15] Guo, X., Y. Liu, and W. Wu, "Wideband unequal filtering power divider with arbitrary constant power ratio and phase difference," *IEEE Transactions on Circuits and Systems II: Express Briefs*, Vol. 70, No. 2, 421–425, 2022.

[16] Zhan, R.-Z. and Y. C. Li, "A wideband high-efficicncy filtering power amplifier," in *2023 IEEE International Workshop on Electromagnetics: Applications and Student Innovation Competition (iWEM)*, 405–407, 2023.

[17] Letavin, D. A., "Compact two-position phase shifter," *Telfor Journal*, Vol. 14, No. 1, 39, 2022.

[18] Feng, L., J. Chen, X. Yu, L. Zhu, and H. Liu, "A novel wideband 90° filtering phase shifter using broadside-coupled MSLs," *IEEE Transactions on Circuits and Systems Ii: Express Briefs*, Vol. 69, No. 6, 2742–2746, 2022.

[19] Zhang, R., B. Yang, Z. Yu, J. Zhou, H. Zhou, and N. Wang, "The low-cost polarization reconfigurable phased array based on high-precision full 360° phase shifter," *International Journal of RF and Microwave Computer-aided Engineering*, Vol. 32, No. 1, e22931, 2022.

[20] Daw, A. F., M. A. Abdalla, and H. M. Elhennawy, "Dual-band divider has rejection band at 5 GHz," *Microwaves and RF Magazine*, 1–6, 2016.

[21] Dong, G., X. Yang, Y. Fang, and M. M. Tenzeris, "Dual-band filtering power amplifier with extended passband bandwidths and wide stopband rejection," *IET Microwaves, Antennas & Propagation*, Vol. 17, No. 9, 749–757, 2023.

[22] Yuan, Y., S. J. Chen, and C. Fumeaux, "Varactor-based phase shifters operating in differential pairs for beam-steerable antennas," *IEEE Transactions on Antennas and Propagation*, Vol. 70, No. 9, 7670–7682, 2022.

[23] Shao, C., H. Chu, X.-H. Zhu, and Y.-X. Guo, "Tunable phase shifter with small phase error and insertion loss fluctuation using a resonator-based structure," *IEEE Transactions on Circuits and Systems II: Express Briefs*, Vol. 70, No. 1, 11–15, 2022.

[24] Khodarahmi, E., M. Elmi, I. M. Filanovsky, and K. Moez, "A 16.5–31 GHz area-efficient tapered tunable transmission line phase shifter," *IEEE Transactions on Circuits and Systems I: Regular Papers*, Vol. 70, No. 4, 1517–1530, 2023.

[25] Ayaz, M., A. Iftikhar, B. D. Braaten, W. Khalil, and I. Ullah, "A composite right/left-handed phase shifter-based cylindrical phased array with reinforced particles responsive to magnetostatic fields," *Electronics*, Vol. 12, No. 2, 306, 2023.

[26] Wang, X.-Z., F.-C. Chen, and Q.-X. Chu, "A compact broadband 4×4 butler matrix with 360° continuous progressive phase shift," *IEEE Transactions on Microwave Theory and Techniques*, Vol. 71, No. 9, 3906–3914, 2013.